PHYSICAL REVIEW B VOLUME 24, NUMBER 6 15 SEPTEMBER 1981

Proton-magnetic-resonance studies of microstructure in plasma-deposited amorphous-silicon—hydrogen films

Jeffrey A. Reimer* and Robert W. Vaughan†
Division of Chemistry and Chemical Engineering, California Institute of Technology, Pasadena, California 91125

John C. Knights
Xerox Palo Alto Research Center, 3333 Coyote Hill Road, Palo Alto, California 94304
(Received 14 January 1981)

Proton-magnetic-resonance data are presented for twenty different plasma-deposited amorphous-silicon—hydrogen films. The two-phase compositional inhomogeneity observed in these films is found to be independent of film thickness down to less than 1 μm. Models for various structural configurations show that these films contain heavily monohydride-clustered regions such as vacancies and voids, as well as $(SiH_2)_n$ and SiH_3 local bonding configurations. The films also contain regions in which monohydride groups are distributed at random. Based on changes in a film whose proton NMR line shapes are metastable as deposited, a model based on strain relief is proposed for film development which explains the ubiquitous presence of the two-phase inhomogeneity. Examination of the changes in proton NMR data as a function of deposition conditions furnishes new insight on the role SiH_2 and SiH_x^+ groups have in models for the gas-phase reactions involved in the developing films. Finally, *p*- or *n*-type doping is found to increase the hydrogen content of the films, and, under heavy *p*-type doping with diborane, boron clustering may occur within the films.

I. INTRODUCTION

Considerable attention has been focused recently on hydrogenated amorphous-silicon (*a*-Si:H) films[1] because of their electronic properties and application to *p*,*n* and Schottky-barrier junctions,[2–4] photovoltaic energy conversion devices,[5] and xerographic photoreceptors.[6,7] There have been several studies on the role that film microstructure plays in determining the electronic properties of the films. In particular, scanning (SEM) and transmission (TEM) electronic microscopy[8] have shown a strong correlation between columnar morphology and the presence of nonradiative recombination centers which limit luminescence efficiency. Small-angle x-ray and neutron scattering results have shown[9,10] that strong isotropic low-angle scattering exists in samples that show no microstructure via TEM or SEM. Vibrational spectroscopy measurements[11–14] have led to the conclusion[12] that growth of columnar microstructure is paralleled by an increase in $(SiH_2)_n$ "polysilane" oscillator strengths.

More recently, proton nuclear magnetic resonance (NMR) data have posed some new questions on the role of hydrogen in structural properties of *a*-Si:H films. Linewidth and line-shape data have shown[15] direct evidence for two-phase compositional inhomogeneity. The two domains differ in the density of hydrogen; however, in both domains the hydrogen nuclei are clustered. Modeling of proton distributions led to the conclusion that the high hydrogen density domain could be due to local clustering on silicon atoms [e.g., $(SiH_2)_n$ "polysilane" regions] or monohydride clustering on internal surfaces. Monohydride clustering was confirmed by further proton NMR studies[16] of annealed *a*-Si:H films. In those studies we showed that upon annealing, hydrogen in the less clustered domain (predominantly monohydride) diffuses internally (prior to evolution) concomitant with the reduction in paramagnetic center density.[17] Further combined NMR and infrared studies on the effects of inert-gas dilution on film formation and growth[18] have shown that high deposition rates achieved with He and Ne diluent gases are associated with levels of hydrogen incorporated in the form of heavily clustered monohydride configurations. Thus, inhomogeneous microstructure occurs not only when $(SiH_2)_n$ is present but when clustered SiH is present as well.

The purpose of this work is to propose structural

models for the proton NMR line shapes and examine the microstructural implications of changing deposition parameters. Specifically, we wish to show (i) saturation experiments which confirm that the two-proton dipolar reservoirs are indeed isolated, (ii) that the two-component behavior of proton NMR line shapes is independent of film thickness (down to 1 μm), (iii) that the two components may be modeled by local bonding configurations and a random distribution of protons, (iv) that hydrogenated vacancies and surfaces are a common microstructural feature, (v) that the spatial isolation of the two-proton domains may be understood in terms of strain in the film during deposition, (vi) that gas-phase chemistry in the discharge influences the microstructural properties of the films, and finally (vii) that p- or n-type doping increases the hydrogen content of the films and heavy p-type doping with diborane may lead to boron clustering within the films.

II. EXPERIMENTAL

Proton-magnetic-resonance data were taken at 56.4 MHz with an NMR spectrometer described previously.[19] The spectra were obtained by Fourier transformation of the free-induction decay (FID) of the magnetization following a preparatory pulse. This usually is a simple 90° pulse, although in the saturation experiments a weak "tickling" field was applied prior to the 90° pulse. The 90° pulse lengths were always less than 2 μsec. In all experiments, the FID's were signal averaged prior to Fourier transformation with 500 acquisitions typically accumulated. Full spin-lattice relaxation was allowed between acquisitions in order to obtain accurate counts of proton spins. The hydrogen content of the films was determined from proton spin counts and sample weight. Spin-lattice relaxation times were measured by the inversion-recovery method.[20] All spectra were least-squares fitted to the sum of a Gaussian component (broad line) and a Lorentzian component (narrow line). The resulting fits were excellent and, based on values of χ^2 resulting from a variety of initial starting parameters, the errors are ± 1 kHz in the FWHM (full width at half maximum) of the broad component (± 0.3 kHz narrow component) and ± 0.3 at. % in the distribution between broad and narrow components.

The samples were prepared in an rf diode deposition described elsewhere.[21] The samples were deposited onto ~ 2-in.-diameter aluminum-foil substrates in thicknesses of ~ 0.1 to 100 μm resulting in sample masses in the range $\sim 0.5-100$ mg after removal of the substrates with a dilute hydrochloric acid etch. Tables I–III detail (i) the deposition conditions for a variety of samples, (ii) the hydrogen content, distribution, and linewidths from the FID spectra, and (iii) the spin-lattice relaxation times.

III. RESULTS

A. Saturation experiments

Figure 1 details the "hole-burning" experiment designed to test the hypothesis that the broad and narrow components of the observed FID spectra are due to spatially isolated dipolar reservoirs. A

TABLE I. Anode films. (RT denotes room temperature.)

Sample	rf[a] power (W)	Substrate temp.	Gas[b] comp.	[H] (at. %) Total[c]	[H] (at. %) Narrow	[H] (at. %) Broad	Linewidth (FWHM, kHz) Narrow	Linewidth (FWHM, kHz) Broad	T_1 (sec)
1	18	RT	5 mol. % Ar	32.3	2.6	29.7	4.7	25.4	2.47
2	2	230 °C	100%	7.8	3.4	4.4	3.8	26.3	2.98
3	1	230 °C	5 mol. % Ar	11.6	3.8	7.8	2.0	26.2	2.01
4	18	230 °C	5 mol. % Ar	12.9	4.5	8.4	1.0	22.4	2.68
5	11	RT	5 mol. % Ar	30.1	2.4	27.7	1.3	26.3	1.80
6	18	230 °C	5 mol. % He	15.8	4.1	11.7	3.0	24.2	3.60
7	2	RT	100%	29.0	3.6	25.4	3.6	27.7	
8	1	230 °C	100%	7.8	3.6	4.2	3.1	31.5	2.48
9	1	230 °C	5 mol. % He	15.1	4.7	10.4	3.5	23.4	
10	18	230 °C	100%	12.6	2.8	9.8	2.8	26.5	

[a]Net into matching network.
[b]Percentage silane in diluent gas.
[c]Determined from integrated spin density and sample weight.

TABLE II. Cathode films.

Sample	rf[a] power (W)	Substrate temp.	Gas[b] comp.	[H] (at. %) Total[c]	Narrow	Broad	Linewidth (FWHM, kHz) Narrow	Broad	T_1 (sec)
11	18	RT	5 mol. % Ar	16.3	2.2	14.1	3.9	22.1	6.02
12	1	RT	5 mol. % Ar	12.6	3.5	9.1	4.7	29.5	7.09
13	18	RT	5 mol. % Ar	15.4	2.0	13.4	2.9	22.2	6.02
14	2	RT	100%	23.1	4.6	18.5	5.4	24.0	
15	18	RT	5 mol. % He	16.5	4.0	12.5	2.3	19.4	4.50

[a]Net in matching network.
[b]Percentage silane in diluent gas.
[c]Determined from integrated proton spin density and sample weight.

weak pulse of magnitude $\omega_1^{sat} \sim 1$ kHz is applied to the sample at frequency ω_{sat} such that $\omega_{sat} - \omega_0 >> \text{FWHM}_{narrow}$ where ω_0 is the center of the narrow component line shape and FWHM_{narrow} is the full width at half maximum of the narrow component. The effect of this pulse is to saturate those components of the line shape that are in rapid (~ 1 msec) spin-spin communcation with those components at ω_{sat}. This saturation pulse is then followed by a short, intense 90° pulse which places the remaining thermally induced magnetization into the x,y plane to be detected by the spectrometer. This is shown schematically in part (a) of Fig. 1. If one compares this experiment to a standard 90° pulse FID measurement [part (b) of Fig. 1] by taking the difference between the standard experiment and the hole-burning experiment, one obtains only the line shape that was saturated by the hole-burning process. The bottom of Fig. 1 shows the results of this experiment for two a-Si:H samples. The figure shows both the FID spectra and the results of the difference experiment. The difference spectra are superimposed on a Gaussian line whose width is given by a best fit to the broad component of the FID spectra. These results show clearly that the broad component of the FID spectra has little spin-spin communication with the narrow component. It is worth noting that moving ω_{sat} to frequency ω_0 results in saturation of both broad and narrow components.

TABLE III. Doped films.

Sample	rf[a] power (W)	Substrate temp.	Gas[b] comp.	[H] (at. %) Total[c]	Narrow	Broad	Linewidth (FWHM, kHz) Narrow	Broad	T_1 (sec)
16	18,*C*	RT	5 mol. % He 1% B_2H_6	14.8	3.1	11.7	2.5	19.2	2.4
17[d]	18,*A*	230 °C	5 mol. % He 1% B_2H_6	14.2	3.3	10.1	4.5	24.2	2.2
18	1,*A*	230 °C	100% 1% PH_3	11.5	4.1	7.4	3.5	31.7	1.4
19	1,*A*	230 °C	100% 1% B_2H_6	8.5	3.1	5.4	2.9	28.3	2.6
20	2,*A*	230 °C	100% 0.1% B_2H_6 0.1% PH_3	9.5	4.0	5.5	3.7	28.1	2.3

[a]Net into matching network. *A* or *C* refers to anode or cathode substrates.
[b]Percentage silane in diluent gas followed by percentage dopant gas.
[c]Determined from integrated proton spin density and sample weight.
[d]A third line is observed in this sample; 0.8 at. % and FWHM 0.79 kHz.

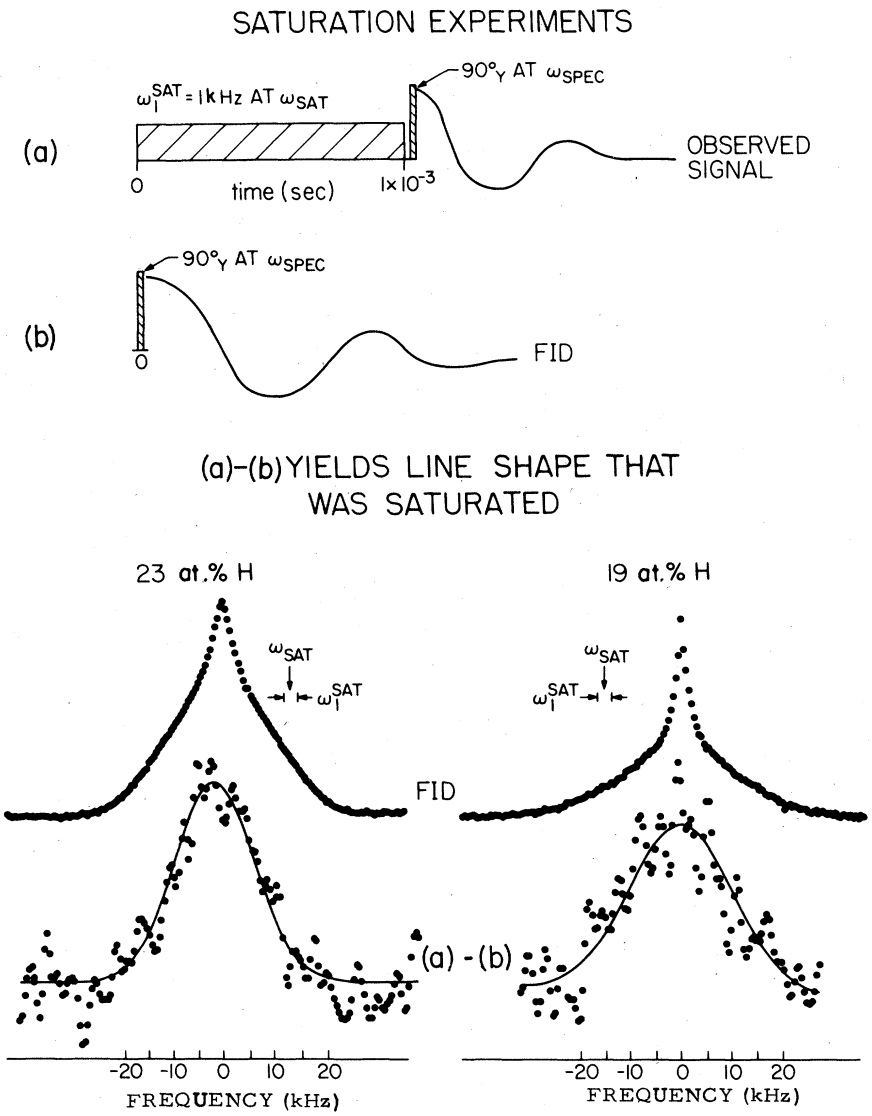

FIG. 1. Schematic diagram (top) of the pulse sequences used in the "hole-burning" experiments. Below, the results for two samples. The dark line in the difference spectra (a)—(b) are Gaussians best fit to the broad component of the FID spectra.

B. Effects of film thickness

A series of samples were prepared by the conditions of sample 6 (Table I), but the total deposition time, hence film thickness, was allowed to vary. The proton FID spectra were obtained for the range 0.1—10 μm in order to determine if proton NMR parameters varied with film thickness. Figure 2 shows the hydrogen content as a function of film thickness over this range as well as the content in the broad and narrow components over the range 1—10 μm. The 0.1-μm sample FID spectrum, while exhibiting two-component behavior, was not deconvolved because of poor signal-to-noise ratio. Figure 2 shows the hydrogen content and distribution to be roughly constant over the 0.1—10 μm range of film thicknesses.

C. Effects of various deposition parameters

Tables I and II show the proton NMR parameters for 15 samples which differ in their deposition parameters. While these data do not represent a systematic survey of the full range of parameters, several trends are worth noting.

(i) In all samples, the hydrogen content in the narrow component is 2—5 at. % (mean, 3.5; standard deviation, 0.8) with linewidth of 1—5 kHz

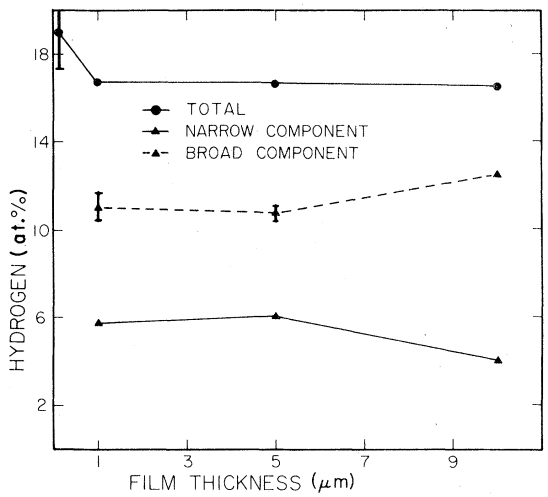

FIG. 2. Changes in the total hydrogen content and the hydrogen content in the broad and narrow components of the proton NMR spectra for films of varying thickness.

(mean, 3.2; standard deviation, 1.0).

(ii) The effect of the diluent gas, notably argon versus helium, may be realized by comparing samples 3 and 9 and samples 4 and 6. These data show the samples deposited in helium have an increased clustering in the narrow component and a higher total hydrogen content. Note in cathode samples, the effects of Ar versus He are negligible.

(iii) The effect of rf power may be realized by comparing samples 3 and 4, 1 and 5, and 12 and 13. For anode samples deposited at high temperatures, the effect of rf power appears to be negligible. For anode samples deposited at room temperature, decreasing rf power causes less clustering in the narrow component and a shorter T_1. For cathode samples, decreasing rf power results in increased clustering of protons in the narrow component and longer T_1's.

(iv) The effects of a diluent gas (Ar or He) vis-á-vis deposition from pure silane may be realized by comparing samples 8, 3, and 9, and samples 10, 4, and 6. The total hydrogen content appears to increase with addition of the diluent gas. In low rf power samples (8, 3, and 9), the increase in hydrogen content is in the broad component.

(v) The effect of substrate temperature on NMR parameters may be realized by comparing samples 1 and 4, and samples 2 and 7. Increasing temperature results in a lower hydrogen content, predominantly reflected in the broad component.

D. Effect of doping with P or B

Table III details the deposition conditions for several samples where dopant gases, diborane or phosphane, were introduced into the deposition system. The effects of doping on the proton NMR parameters may be summarized as follows.

(i) In 100 mol.% SiH_4 anode samples deposited at 230 °C (compare samples 18 and 19 from Table III with sample 8 from Table I), the hydrogen content increases when either PH_3 or B_2H_6 is introduced. The phosphorus-doped sample has a shorter T_1 than the boron-doped sample.

(ii) In 5 mol. % SiH_4 in helium samples (anode) deposited at 230 °C (compare sample 17 from Table III with sample 6 from Table I), introduction of diborane reduced the T_1.

The proton FID spectrum of this doped sample 17 is complicated by an additional broad ($\sim$ 50 kHz FWHM) and narrow component (800 Hz FWHM). The narrow component is temperature dependent (Fig. 3) such that reducing the temperature broadens the narrow component to the point where it appears to lack any contribution to the observed spectrum. The total hydrogen content in the additional broad and narrow component, however, is less than $\sim$2 at. %.

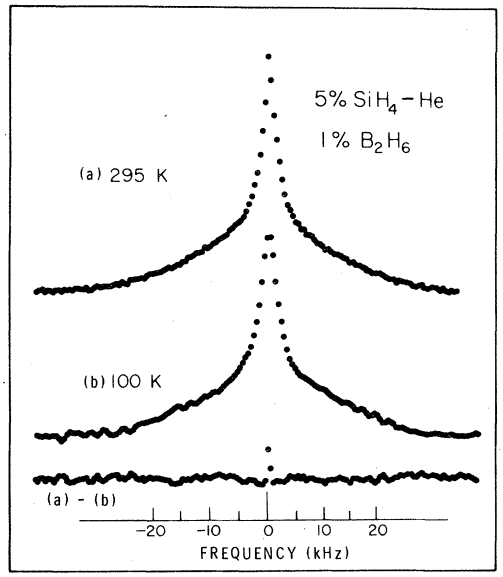

FIG. 3. Room-temperature and low-temperature proton NMR spectra for a heavily doped p-type a-Si:H film. At the bottom is the difference (room temperature − 100 K) of the two spectra, which clearly shows the motionally narrowed component in the room temperature spectrum.

E. Effects of time on a high defect density sample

A high defect density sample ($> 10^{19}$ spins/cm^3) was prepared by depositing from 5 mol. % SiH_4-Ar at 25 °C with an rf power of 18 W. Figure 4 compares the proton FID spectra of the sample freshly deposited[1] with the FID spectra of the same sample allowed to stand in dry air for approximately six months. As deposited, the NMR spectra yields the hydrogen content to be 23.8 at. % and 18.1 at. % broad (25.8 kHz FWHM), 5.0 at. % narrow (1.65 kHz FWHM), and ~ 1.5 at. % very narrow (~ 1 kHz FWHM). The proton spectrum of the "aged" sample yields 29.5 at. % H with 20.9 at. % broad (26.8 kHz FWHM) and 3.7 at. % narrow (2.8 kHz FWHM).

IV. DISCUSSION

A. Structural models for *a*-Si:H

Having established that the proton NMR line shapes are dipolar broadened,[15] and that the two components are indeed spatially isolated (Fig. 1), we may consider specific structural features which may give rise to these observed line shapes. It is well known that the second moment (M_2) of a dipolar-broadened spectrum in an amorphous material is given by[22]

$$M_2 = \tfrac{3}{5}\gamma^4\hbar^2 I(I+1)\sum_{j,k} r_{kj}^{-6}\,, \qquad (1)$$

where γ is the proton gyromagnetic ratio, I the value of nuclear spin ($\frac{1}{2}$ for protons), and $\sum_{j,k} r_{kj}^{-6}$ represents a lattice sum of distances to other proton nuclei. Following our earlier work,[15] we shall apply Eq. (1) to two types of models. The first, using Eq. (1) directly, models local bonding configurations of hydrogen on silicon such as SiH_3 groups, etc. The second model is used to calculate the second moment of a known number of spins dispersed on a simple cubic lattice.

Table IV shows the results of applying Eq. (1) to various local bonding configurations. Given the sensitivity of the calculations to slight changes in interatomic distances, we make only general comments. The hydrogenated monovacancy model yields a linewidth much larger than those observed and based on the sensitivity of the NMR experiment we conclude that there is less than 0.1 at. % hydrogen associated with monovacancies and divacancies ($< 10^{18}$ per cm^3). This is consistent with the knowledge that monovacancies in crystalline silicon are not stable.[23] All of the other configurations shown in Table IV may give rise to the broad component and their presence would be dependent upon the deposition conditions. Of particular interest is the persistence of the broad component in samples which show no microstructure by small-angle x-ray and neutron scattering experiments[9] (note samples 2, 8, 9, 18, 19, and 20 in Tables I and III). In addition, these samples show predominantly monohydride signatures in their vibrational spectra. Table IV shows that hydrogenated trivacancies, etc., may yield the broad component,

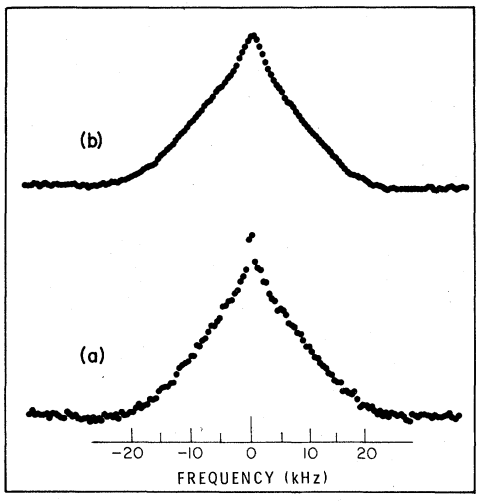

FIG. 4. Proton NMR spectra for (a), a freshly deposited *a*-Si:H sample (RT, 18 W, 5 mol. % SiH_4-Ar, anode), and (b) for the same sample after exposure to dry air for about six months.

TABLE IV. Broad linewidth calculations.

Configuration	Full width at half maximum[a] (kHz)
SiH_2[b]	13.6
$(SiH_2)_n$	17.1
SiH_3	19.2
c-Si (surface) (hydrogenated)	9–60
c-Si monovacancy (hydrogenated)	90.2
c-Si divacancy (hydrogenated)	68.7
observed[c]	25.4±3.4

[a]Calculated using Eq. (1).
[b]SiH_2 will give rise to a Pake doublet. However, in the amorphous matrix the doublet components will be expected to broaden to the point where no structure will be observed in the spectrum.
[c]Mean and standard deviation of the values in Tables I–III.

and at least the trivacancies would probably be beneath the detection limits as a void by the scattering experiments (although small isotropic scattering persists in many samples).[24] In samples such as 8 (Table I), where only monohydride vibrational spectra are observed, the 4.2 at. % hydrogen in the broad component would correspond to a "trivacancy density" of approximately 1.8×10^{20} cm^3 or an average separation between trivacancies of about 18 Å (assuming the density of *a*-Si:H is 2 g/cm^3). Note that once the deposition conditions are changed so that SiH_x ($x > 1$) vibrational bands are observed and/or larger scale microstructure appears, a variety of configurations may give rise to the broad component.

To model the protons responsible for the narrow component, we consider the modification of Eq. (1) to the configuration a simple cubic lattice[22]:

$$M_2 = 5.1\gamma^4\hbar^2 I(I+1)d^{-6}\,, \tag{2}$$

where d is the lattice constant (and nearest-neighbor distance). We then take the known hydrogen content in the narrow component and disperse it homogeneously throughout the fraction of the film not occupied by the broad component (plus some buffer region to assure spatial isolation of the two dipolar reservoirs). The inverse cube root of the resulting spin density yields a value for d which, when inserted into Eq. (2), yields a value for M_2 which may be compared with experiment. Figure 5 shows the experimentally observed narrow component linewidth (mean and standard deviation of the samples shown in Tables I—III), and the predicted linewidth for a homogeneous distribution of the known hydrogen content in the narrow component (mean and standard deviation in Tables I—III), assuming 25% of the *a*-Si lattice is excluded due to the broad component protons and buffer region. The discrepancy between the model linewidths and the observed linewidths shown in Fig. 5 has led previously[15,25(a)] to the conclusion that the narrow component is predominantly clustered monohydride.

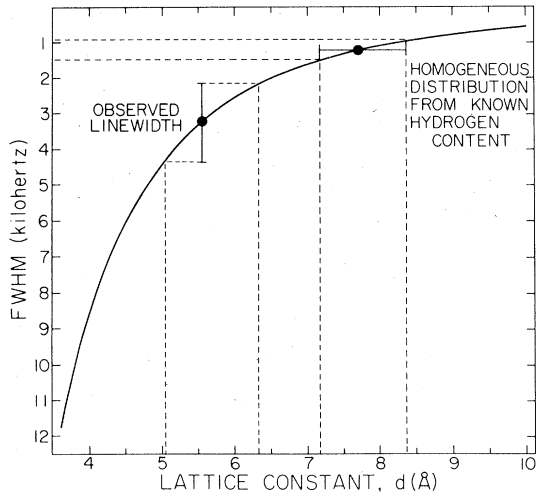

FIG. 5. Schematic diagram, from Eq. (2) in the text, showing that a homogeneous distribution of protons in the narrow component of the proton NMR spectrum will not give rise to the observed linewidths. The points and error bars are the mean and standard deviation of the linewidths and hydrogen content of the narrow components of 15 different *a*-Si:H samples.

Since this narrow component has nearly the same hydrogen content (3.5 ± 0.8 at. %) and linewidth (3.2 ± 1 kHz) in all films, including those which show only monohydride vibrational spectra, we conclude that the narrow component is due only to monohydride species. However, the observed broadening may be explained by considering a *random* distribution of proton spins rather than a *clustered homogeneous* (cubic lattice) distribution. We modify the lattice sum in Eq. (1) with a probability distribution $P(r)$

$$M_2 = A\int_{r_i}^{r_f} r^{-6}P(r)dr\,, \tag{3}$$

where A is the usual collection of fundamental constants, and r_i and r_f minimum and maximum distances considered. We assume a Gaussian distribution

$$P(r) = \exp\frac{-(r-r_0^2)}{2\Delta^2} \tag{4}$$

of distances about the r_0 determined from the inverse cube root of the spin density. Inspection of Fig. 5 yields $r_0 = 7.7$ Å and numerical solution of Eq. (3) shows that when $\Delta = 1.7$ Å, we get an excellent match of the observed linewidth with the random-distribution model. Therefore, we conclude that the narrow component is due to monohydride groups distributed at random in the *a*-Si lattice.

An important structural parameter is the dimensions of the buffer region between the high and low hydrogen density domains (broad and narrow linewidths, respectively). A minimum distance would be given by the average separation between protons in the narrow component since the broad component protons have a T_2 roughly eight times shorter than the narrow component protons. This places a minimum of 5—6 Å on the width of the buffer zone between the high-density hydrogen region and low-density region. In sample 8 (Table I), we estimated previously a trivacancy density of

1.8×10^{20} cm^3, and assuming a 5—6 Å buffer region, we calculate that 5—30 % of the *a*-Si lattice is taken up by high hydrogen density and buffer zone regions, in reasonable agreement with the modeling shown in Fig. 5.

The assignment of the broad component to structural inhomogeneities [voids, vacancies, $(SiH_2)_n$ regions, etc.] and the narrow component to interstitial monohydride groups provides a natural explanation as to why the hydrogen relaxation center density, responsible for proton spin-lattice relaxation,[25(a)] is higher for the narrow component protons than the broad component protons.[25(b)] The narrow component protons "feel" the fluctuating fields due to a three-dimensional distribution of relaxation centers whereas protons situated on a void see a lower dimensionality distribution of relaxation centers (i.e., protons on void surfaces as opposed to those in the bulk). Hence, the narrow component protons would be expected to relax faster (under conditions of homonuclear dipolar interaction suppression[25(b)]) than the broad component protons.

The observation of this two-phase compositional homogeneity presents another interesting question: Is the structure of these films determined by surface-bulk processes during deposition or by gas-phase reactions? We shall argue that, in fact, both factors influence film microstructure. However, the persistence of the two-phase structure as seen by NMR, regardless of the deposition conditions, would imply a bulk or surface rearrangement of the film after nucleation. To test this hypothesis, we prepared a high unpaired spin density ($>10^{19}$ cm^{-3}), high hydrogen content *a*-Si:H sample and recorded the NMR spectrum just after deposition and then recorded the spectrum six months later. As Fig. 4 illustrates, the hydrogen content and distribution appears to undergo rearrangement. It has been shown previously[25(b)] by NMR relaxation data that the hydrogen content of this fresh sample, as determined by NMR line shapes, is artificially low ($\sim$8 at. %) because of large dipolar broadening of the hydrogen spins by the abundant unpaired electrons. Nonetheless, we propose that the "stabilization" process shown in Fig. 3 may serve as a model for what may happen during film growth, namely, hydrogenation of dangling and strained bond interfaces by diffusion of hydrogen from other regions in the lattice. We then picture areas of high strain during film growth as "gettering" the hydrogen out of the immediately surrounding lattice and forming a hydrogenated void (or surface), thereby stabilizing the lattice and spatially isolating the hydrogen in the void from that in the bulk. It is worth noting that during growth of films in which there are $(SiH_2)_n$ polymer phases, the same process may occur with the polymer phase playing the same role as the hydrogenated void: a mechanism by which the strain in the continuous random network is relieved. Finally, we should comment on the role oxygen may play in the stabilization process shown in Fig. 4. Studies on sputtered *a*-Si:H films have shown that oxygenated films have remarkably different photoconductivity, photoluminescence, and optical absorption properties.[26] However, a recent study[27] of plasma-deposited films has shown that changes in optical absorption and luminescence data occur monotonically with addition of oxygen. Furthermore, in samples in which there was up to 0.1 at. % oxygen in the silane during deposition, there was observed to be no change in ESR data. Hence, we conclude that some oxygen may have been incorporated in the film shown in Fig. 4 over time, but is not responsible for the observed changes in hydrogen distribution.

B. Effects of film thickness

Figure 2 shows that the microstructure and hydrogen content of *a*-Si:H films are roughly constant to as thin as the submicrometer level. There have been several recent studies[28—32] on the effects of film thickness on optical properties[30—32] and hydrogen content.[28,29] Nuclear activation reaction techniques[28] have shown that the hydrogen content decreases within 0.1 μm of an interface for some samples,[29] and increases for others.[28] Unfortunately, the data reported herein have insufficient signal-to-noise ratios to study thicknesses on the order of 0.1 μm. However, the use of superconducting solenoids and/or lower temperatures would allow proton NMR studies of samples with $\sim1\times10^{17}$ proton spins, or about 100—1000-Å films prepared with our deposition apparatus.

C. The influence of deposition conditions on NMR parameters

While all the samples reported herein have two-component proton NMR spectra, there are considerable variations among the samples as to the atomic percent of hydrogen, particularly the atomic percent of hydrogen contained within the broad component. We wish to point out the trends in these proton data *(vide supra)* may be understood in terms of some gas-phase reactions and mechanisms for film growth.

There have been several papers published recently which propose mechanisms for film growth and gas-phase chemistry.[33–39] These papers include structural studies of the films,[33] films prepared from higher molecular weight silanes,[37] mass spectroscopy of the glow discharge,[36,39] optical absorption studies of the glow discharge,[34,35] and effects of inert gas dilution of the silane.[38] The consensus of these works is that SiH_2 and/or SiH_3 groups are responsible for film growth, for example,[37]

$$n[SiH_2(g)] \rightarrow SiH_x(s) + SiH_4(g) + H_2(g) \ . \quad (5)$$

The role ionic species play is somewhat clouded. A recent model,[38] used to explain the differences between films deposited in Ar or Kr versus He or Ne, proposed that ions "scour" the surface of the growing film and thus remove segments of $(SiH_2)_n$ chains formed on the surface. We wish to propose that Eq. (5) and the "scouring theory" are sufficient to explain the trends (ii)—(v) discussed in Sec. III.

Consider the data for films 8, 3, and 9 (Table I) which compare the effects of deposition from pure silane, 5 mol. % in Ar, and 5 mol. % silane in He. The deposition rates for these films are in the order 100% SiH_4 < 5 mol. % SiH_4-Ar < 5 mol. % SiH_4-He. Inspection of Eq. (5) shows that more $SiH_2(g)$ or less $H_2(g)$ will provide for faster growth of the film. Mass spectroscopic studies[36,39] have shown the concentration of $H_2(g)$ to be higher in the pure SiH_4 deposition than deposition from Ar, consistent with Eq. (5) and the deposition rates. The observed increase in hydrogen content in the films over this same trend may be the result of trapping of hydrogen in the growing film; i.e., faster film growth implies more H is trapped in the growing film. This faster growth implies a more strained *a*-Si lattice which in turn is relaxed by the formation of vacancies or other microstructural features. Accordingly, faster deposition rates would imply an increase in the broad component in the NMR spectra, consistent with the observed data. Whether or not the broad component corresponds to vacancies or to $(SiH_2)_n$ regions, larger voids, cracks, etc., depends on the availability of ions (SiH_x^+) to "scour" the surface. As discussed previously,[38] deposition in He or pure SiH_4 results in higher ion densities (more scouring) than deposition in Ar because Ar has a metastable energy less than the ionization potentials of SiH_x, ($x = 1-3$) and thus absorbs most of the plasma electron energy. Hence, films deposited in He and pure SiH_4 have only monohydride signature in their vibrational spectra and finer scale inhomogeneities as seen by electron microscopy (broad component is the trivacancies, surfaces, etc.)

The dependence of the films deposited from 100 mol. % SiH_4, 5 mol. % SiH_4-Ar, and 5 mol. % SiH_4-He on rf power is worth considering in light of these models for film growth. Samples 10, 4, and 6 represent the same deposition conditions as 8, 3, and 9 except the rf power has been increased from 1 to 18 W. The samples deposited from 5 mol. % SiH_4 in He or Ar show little changes in their NMR spectra yet the sample deposited from pure SiH_4 shows an increase in the broad component and the deposition rate. We suggest that the availability of $(SiH_2)(g)$ is increased with increasing rf power in pure SiH_4 deposition, whereas this effect is mediated in the inert gas mixtures as the metastables of the inert gas atoms are responsible for absorption of most of plasma energy.

The scouring of the developing film surface by ions should be affected by magnetic or electric fields and temperature. An increase in substrate temperature would presumably result in increased mobility of $(SiH_2)_n$ groups on the surface and hence allow for more effective scouring. Furthermore, increasing the substrate temperature would shift Eq. (5) to the left, slowing film growth. Hence, we expect higher substrate temperatures to decrease the total hydrogen content and minimize large-scale microstructure and $(SiH_2)_n$ formation. This is consistent with these proton NMR data as well as microstructural studies[10,11,33] [compare samples 7 with 2, as well as 1 with 4 (Table I)]. Samples deposited on cathode substrates have a large negative dc bias which would increase the ion flux rate at the developing film surface. These NMR data are consistent with this concept as the effects of Ar versus He diluent gas (i.e., the ion concentration) on NMR parameters is negligible on cathode substrates (samples 11 and 15 in Table II). This may explain trends in the recent literature on the effects of electric and magnetic fields on *a*-Si:H deposition.[40–42]

D. The effects of doping on the observed NMR parameters

A recent study[31] of the hydrogen content of phosphorus (*n* type) and boron (*p* type) doped *a*-Si:H films via nuclear activation techniques has shown that the Fermi level position varies linearly with the hydrogen content. Their reported values of the hydrogen content range from ~4 at. % for highly *n*-type films to ~10 at. % for highly *p*-type materials (intrinsic values of ~7.5 at. %). Other

workers[43] have not shown a linear dependence. Inspection of our data for samples 18, 19 (Table III), and 8 (Table I) may be compared to the nuclear activation study[31] since the deposition conditions are roughly comparable. Our data show both the *n*-type and *p*-type material to increase in hydrogen content relative to the intrinsic material, with the largest increase observed for phosphorus (*n*-type) doping. The reason for the discrepancy between our data and the Dundee group nuclear reaction results is unclear, perhaps being due to differences in the deposition apparatuses. It is worth noting, however, that both B_2H_6 and PH_3 are expected to absorb electron energies[44] less than 11 eV from the plasma and may influence the ion concentrations, deposition rates, and hydrogen content in a similar fashion as Ar and Kr diluent gases. The data from Table III are consistent with the Ar diluent gas effects.

Figure 3 shows that when deposited in helium, high *p*-type doping results in a motionally narrowed component in the proton NMR spectrum. An analysis of the FID prior to Fourier transformation shows a small broad component ($\sim$50 kHz) in the spectra as well. We attribute these proton spectra to protons experiencing an amorphous-boron-type environment. Previous proton NMR studies[45] have shown that *a*-B:H films deposited from B_2H_6 in helium yield two-component spectra where one component is motionally narrowed and the broad component is further broadened beyond that expected from H-H dipolar interactions by heteronuclear ($^{10}B/^{11}B$) dipolar interactions. We conclude that some boron clustering is present under 5 mol. % SiH_4-1 mol. % B_2H_6-He deposition conditions. This implies that boron preferentially bonds to other boron neighbors during film growth at high boron doping levels.

V. SUMMARY AND CONCLUSIONS

In summary, we have presented proton NMR spectra for *a*-Si:H films under a variety of deposition conditions. The two-component line shapes observed in all spectra are modeled in terms of local bonding configurations, and both homogeneous and random distributions of protons. The heavily clustered phase (broad component) corresponds to those protons associated with microstructure such as voids, hydrogenated surfaces, and polysilane regions. In films which show predominantly monohydride vibrational spectra, small voids such as trivacancies or surfaces may give rise to the broad component with a minimal number of monovacancies and divacancies. The lightly clustered phase (narrow component) is predominantly composed of monohydride groups that are distributed randomly throughout the film. The spatial separation of the broad and narrow component protons may arise from regions of high strain during film growth "gettering" hydrogen nuclei out of the neighboring *a*-Si lattice and forming hydrogenated voids which in turn relieve local strain. We have shown that this is the case in at least one sample which, as deposited, was "metastable" and microstructural changes, via the NMR line shapes, were found to occur with time. The two-domain proton inhomogeneity was found to be independent of film thickness down to 1 μm. Furthermore, changes in the details of the NMR line shapes as a function of deposition conditions have been described in terms of film formation from SiH_2 gas-phase species and film scouring due to the presence of SiH_x^+ ions. Finally, we have shown that doping of the films, either *p* type or *n* type, results in an increase in the total hydrogen content of the films, and when high boron levels are present in the gas phase, boron clustering occurs within the films.

We conclude that proton NMR line shapes are useful probes of the hydrogen distribution in *a*-Si:H films. More experiments are required to better understand the relationship between gas-phase chemistry and film properties as well as the relationship between NMR parameters and optical properties.

ACKNOWLEDGMENTS

The authors wish to thank R. A. Lujan for his expert assistance with sample preparations, and Dr. S. I. Chan and Dr. T. M. Duncan for their help in preparing this manuscript. Also, we thank James Gleeson, Dave Biegelsen, and Marc Brodsky for helpful discussions. This work was supported by the National Science Foundation under Grant No. DMR-77-21394 and the Solar Energy Research Institute under Contract No. XJ-0-9079-1.

*Current address: IBM T. J. Watson Research Center, Yorktown Heights, New York 10598.
†Deceased.

[1(a)]*Amorphous Semiconductors,* Vol. 36 of Topics in Applied Physics, edited by M. H. Brodsky (Springer, Berlin, 1979); (b) D. E. Carlson, C. R. Wronski, J. I. Pankove, P. J. Zanzucchi, and D. L. Staebler, RCA Rev. 38, 211 (1977).

[2]W. Paul, A. J. Lewis, G. A. N. Connell, and T. D. Moustakas, Solid State Commun. 20, 969 (1976); G. A. N. Connell and J. R. Pawlik, Phys. Rev. B 13, 787 (1976).

[3]W. F. Spear, P. G. LeComber, S. Kimmond, and M. H. Brodsky, Appl. Phys. Lett. 28, 105 (1976).

[4]D. E. Carlson and C. R. Wronski, Appl. Phys. Lett. 28, 671 (1976).

[5]E. E. Carlson, IEEE Trans. Electron Devices ED-24, 449 (1977).

[6]I. Shimizu, T. Komatsu, K. Saito, and E. Inoue, J. Non-Cryst. Solids 35, 773 (1980).

[7]J. Mort, S. Grammatica, J. Knights, and R. Lyan, Solar Cells 2, 451 (1981).

[8]J. C. Knights and R. A. Lujan, Appl. Phys. Lett. 35, 244 (1979).

[9]A. J. Leadbetter, A. A. M. Rashid, R. M. Richardson, A. F. Wright, and J. C. Knights, Solid State Commun. 33, 973 (1980).

[10]P. D'Antonio and J. H. Konnert, Phys. Rev. Lett. 43, 1161 (1979).

[11]M. H. Brodsky, M. Cardona, and J. J. Cuomo, Phys. Rev. B 16, 3556 (1977).

[12]G. Lucovsky, R. J. Nemanich, and J. C. Knights, Phys. Rev. B 19, 2064 (1979).

[13]W. Paul, Solid State Commun. 34, 283 (1980).

[14]H. Shanks, C. J. Fang, L. Ley, M. Cardona, F. J. Demond, and S. Kalbitzer, Phys. Status Solidi B 100, 43 (1980).

[15]J. A. Reimer, R. W. Vaughan, and J. C. Knights, Phys. Rev. Lett. 44, 193 (1980).

[16]J. A. Reimer, R. W. Vaughan, and J. C. Knights, Solid State Commun. 37, 161 (1981).

[17]D. K. Biegelsen, R. A. Street, C. C. Tsai, and J. C. Knights, Phys. Rev. B 20, 4839 (1979).

[18]J. C. Knights, R. A. Lujan, M. P. Rosenblum, R. A. Street, D. K. Biegelsen, and J. A. Reimer, Appl. Phys. Lett. 38, 331 (1981).

[19]R. W. Vaughan, D. D. Elleman, L. M. Stacey, W. K. Rhim, and J. W. Lee, Rev. Sci. Instrum. 43, 1356 (1972).

[20]T. C. Farrar and E. D. Becker, *Pulse and Fourier Transform NMR* (Academic, New York, 1971).

[21]R. A. Street, J. C. Knights, and D. K. Biegelsen, Phys. Rev. B 18, 1880 (1978).

[22]A. Abragam, *The Principles of Nuclear Magnetism* (Clarendon, Oxford, England, 1961).

[23]W. E. Spear and P. G. LeComber, Philos. Mag. 33, 935 (1976).

[24]J. C. Knights, J. Non-Cryst. Solids 35/36, 159 (1980).

[25](a) W. E. Carlos and P. C. Taylor, Phys. Rev. Lett. 45, 358 (1980); (b) J. A. Reimer, R. W. Vaughan, and J. C. Knights, Phys. Rev. B 23, 2567 (1981).

[26]M. A. Paesler, D. A. Anderson, E. C. Freeman, G. Moddel, and W. Paul, Phys. Rev. Lett. 41, 1492 (1978).

[27]J. C. Knights, R. A. Street, and G. Lucovsky, J. Non-Cryst. Solids 35/36, 279 (1980).

[28]M. H. Brodsky, M. A. Frisch, J. F. Ziegler, and W. A. Lanford, Appl. Phys. Lett. 30, 561 (1977).

[29]D. G. Ast and M. H. Brodsky, Philos. Mag. B 41, 273 (1980).

[30]D. G. Ast and M. H. Brodsky, J. Non-Cryst. Solids 35/26, 611 (1980).

[31]G. Müller, F. Demond, S. Kalbitzer, H. Damjantschitsch, W. E. Spear, P. G. LeComber, and R. A. Gibson, Philos. Mag. B 41, 571 (1980).

[32]I. Solomon and M. H. Brodsky, J. Appl. Phys. 51, 4548 (1980).

[33]J. C. Knights, J. Non-Cryst. Solids 35/36, 159 (1980).

[34]P. Kocian, J. Non-Cryst. Solids 35/36, 195 (1980).

[35]A. Matsuda, K. Nakagawa, K. Tanaka, M. Matsumura, S. Yamasaki, H. Okushi, and S. Iizima, J. Non-Cryst. Solids 35/36, 183 (1980).

[36]G. Turban, Y. Catherine, and B. Grolleau, Thin Solid Films 67, 309 (1980).

[37]B. A. Scott, M. H. Brodsky, D. C. Green, P. B. Kirby, R. M. Plecenik, and E. E. Simonyi, Appl. Phys. Lett. 37, 725 (1980).

[38]J. C. Knights, R. A. Lujan, M. P. Rosenblum, R. A. Street, D. K. Biegelsen, and J. A. Remier, Appl. Phys. Lett. 38, 331 (1981).

[39]G. Turban, Y. Catherine, B. Grolleau, Thin Solid Films 77, 287 (1981).

[40]M. Taniguchi, M. Hirose, and Y. Osaka, J. Non-Cryst. Solids 35/36, 19 (1980).

[41]H. Okamoto, T. Yamaguchi, Y. Nitta, and Y. Hamakawa, J. Non-Cryst. Solids 35/26, 201 (1980).

[42]L. J. Dimmey, P. L. Jones, and F. H. Locks, Thin Solid Films 67, L13 (1980).

[43]I. Haller and M. H. Brodsky, in *Physics of Semiconductors 1978,* edited by B. L. H. Wilson (Institute of Physics, London, 1979), p. 1147.

[44]G. Herzberg, *Molecular Spectra and Molecular Structure III: Electronic Spectra and Electronic Structure of Polyatomic Molecules* (Van Nostrand Reinhold, New York 1966) shows that both ionization potentials and B—H (or P—H) bond dissociation energies are less than 11 eV.

[45]J. A. Reimer, R. W. Vaughan, J. C. Knights, and R. A. Lujan, J. Vac. Sci. Technol. 19, 53 (1981).